DOI: 10.5281/zenodo.4292694

Use of FTIR spectroscopy of pyridine adsorption at incipient moisture conditions in the interpretation of the hydrophobicity, acidity, and activity on HMOR and HY zeolites

Uso de la espectroscopía FTIR de adsorción de piridina en condiciones de humedad incipientes en la interpretación de la hidrofobicidad, acidez y actividad en zeolitas HMOR y HY

Luis F. Isernia-Trebols
Laboratorio de Tamices Moleculares, Universidad de Oriente, Venezuela. E-mail: luis.isernia@gmail.com

Recibido 21/11/2019
Aceptado para publicación 15/11/2020

Abstract

The fatty acids (FFA) adsorption on structurally different (HMOR and HY) zeolites with different Si/Al ratios, were studied by FTIR pyridine spectroscopy on incipient moisture conditions and other complementary characterization techniques to improve the understanding of the relationship between hydrophobicity, acidity, and activity. In HMOR with a low density of Si-OH–Al groups, a significant fraction of the FFA molecules are adsorbed onto the less polar sites with its carboxyl groups oriented away from the surface. In HY, the higher density of bridging Si-OH–Al groups, favors the adsorption of FFA molecules with their carboxyl group hydrogen-bonded to these groups.

Keywords: Acidity, FTIR, pyridine, hydrophobicity, mordenite, faujasite.

Resumen

Se estudiaron zeolitas estructuralmente diferentes (HMOR y HY) mediante espectroscopia FTIR-piridina bajo humedad incipiente y técnicas complementarias. Con la salida del aluminio tetraédrico de la red cristalina aumenta la hidrofobicidad y disminuyen la acidez y la actividad. A crecientes relaciones Si/Al, en mordenitas con baja densidad de sitios Si-OH-Al las moléculas de ácidos grasos se adsorben crecientemente sobre sitios menos polares con sus colas orientadas hacia la superficie. En las faujasitas, su mayor densidad de sitios en puente favorece la adsorción de los ácidos grasos, con sus carboxilos orientados hacia los sitios Si-OH-Al, disminuyendo su adsorción a relaciones Si/Al crecientes.

Palabras clave: FTIR, piridina, hidrofobicidad, mordenita, faujasita.

Highlights

1. The FTIR/pyridine spectroscopy on incipient moisture conditions was employed.
2. Steam dealumination was applied on HMOR and HY (Si/Al ≈ 6 and 3) at 800 and 1000 K.
3. Hydrophobicity increases with the dealumination, but the acidity diminishes.

DOI: 10.5281/zenodo.4292694

4. In the HMOR series, hydrophobicity drives the adsorption by the London forces.

5. In HY series, acidity drives the adsorption of the fatty acids through H-bonding.

Graphical Abstract / Resumen gráfico

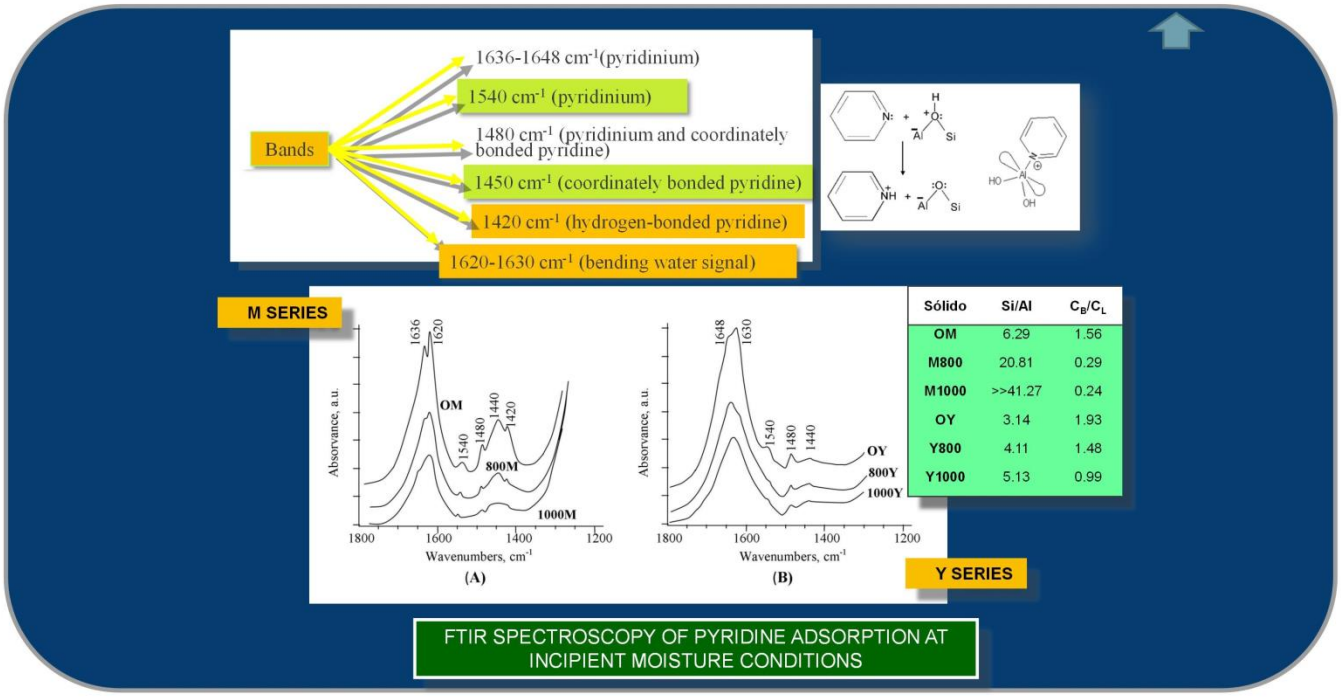

1. Introduction

In zeolites, the hydrophobicity has a direct relationship with their energetic selectivity [1] originated by the electrostatic forces between the zeolitic structure and the molecules that come into the intra-crystalline space; turning the hydrophobicity in one of the most influential properties over the catalytic activity. The hydrophobicity drives the selective adsorption, affecting positively or negatively the adsorption forces and the number of adsorbed polar and unsaturated molecules. In this sense, it can also act selectively on amphipathic molecules, as the free fatty acids. Moreover, stands out the relationship usually opposite between the hydrophobicity and the acidity, taking into account that acid sites of the zeolitic catalysts usually are an active part of the catalysis.

Aluminum segregation outside the crystalline framework, through dealumination treatments, is a frequent cause of the structural collapse [1,2] with the resulting change of the catalyst's physical-chemical properties and the activity. Then, the crystallinity of zeolites has a direct relationship with the presence of tetrahedral aluminum, which is the main responsible for the Brönsted acidity [1,2]. Between the diverse analytical techniques, the Fourier transform infrared (FTIR) spectroscopy has an important use in catalysts characterization due to its capacity to provide essential information without destroying the matrix. On the other hand, the use of special cells allows tracking the changes occurring in the IR bands of basic probes, adsorbed on the catalyst acid sites, due to changes in the nature of these sites. For example, pyridine adsorption generates a series of signals, among which two are prominent [3,4,5]: one signal around 1545 cm^{-1} (pyridinium ion bonded to a Brönsted site) and another near 1455 cm^{-1} (coordinately bonded pyridine).

DOI: 10.5281/zenodo.4292694

This work approaches the use of the FTIR spectroscopy of pyridine adsorption on incipient moisture conditions and other complementary characterization techniques on the interpretation of insufficiently clarified questions regarding the effect of the leaving of tetrahedral aluminum out of the crystalline network on the hydrophobicity and the creation and disappearance of adsorption sites; as well as the effect of the zeolite topology and density of bridging Si-OH–Al groups on the manners of adsorption of free fatty acid (FFA) molecules; and the nature of the primary factors that promote the activity in the esterification of FFA on structurally different zeolites with different Si/Al ratios.

2. Experimental

The original HMOR zeolite (labeled OM), was obtained from 9 g of sodium mordenite (Union Carbide, Si/Al ratio of about five) through exhaustive ion-exchange for 24 h under agitation with 250 mL of 40% NH_4NO_3 aqueous solution at a boiling temperature in a reflux assembly. Then, the exchanged ammonium–mordenite was filtered by suction and washed with 2200 mL of distilled water, in portions of 500 mL. The resulting solid was then dried in a stove to 373 K for 24 h and calcined up to 803 K for 4 h, to yield the protonated-zeolite (OM). Portions of 0.4 g of OM were hydrothermally treated at 800 and 1000 K for 120 min with 100 % steam. According to the treatment temperature the resulting solids were designated as M800 and M1000. The same treatment was applied to a NaY zeolite (Union Carbide, Si/Al ratio of about three) yielding the OY, Y800, and Y1000 solids. The solid-state ^{29}Si and ^{27}Al NMR characterizations were made in a Bruker AVANCE/300 MHz/7.0 T equipment. For the MAS-NMR studies, zeolite samples from 200 to 300 mg were subjected to ^{29}Si (59.62 MHz) and ^{27}Al (78.20 MHz) at 7.0 T referred to TMS and $Al(NO_3)_3$ respectively. The ratio Si/Al was calculated from the intensity of the signals $I_{Si(nAl)}$ [2] by the Eq. (1):

$$(Si/Al)_{RMN} = \frac{\sum_{n=0}^{4} I_{Si(nAl)}}{\sum_{n=0}^{4} 0.25 n I_{Si(nAl)}} \quad (1)$$

The XRD study was performed in a Siemens D5005 diffractometer with a θ/θ geometry in a reflection mode, equipped with a graphite secondary monochromator, in the 2θ range of 5–70° and 0.02° steps of 1.5 s. Cu K_α (λ=1.54056Å) radiation, working at 40 kV and 30 mA. The density of acid sites and their strengths distribution was determined by the TPD-NH_3 methodology, through a TPD system laboratory-constructed. The analysis was based on previously outlined guidelines [3] with selective detection of NH_3. Each of the samples (100 mg) was previously pulverized in an agate mortar and activated in a quartz reactor at 873 K, under a 50 mL/min flow of dry N_2 at 101 kPa for one hour. After the cooling at room temperature under a flow of dry N_2, the samples were saturated with NH_3 (50 mL/min and 101 kPa) for 15 minutes. The excess of NH_3 was eliminated with a 50 mL/min N_2 flow until there was no detection of NH_3. Then the TPD experiments were performed with a continuous N_2 flow (50 mL/min) and heating rate of 10°C/min until 873 K. The nature of the existing acid sites in both zeolite series was examined through FTIR spectroscopy of pyridine adsorption, on solids submitted to incipient moisture conditions, trying to reproduce the conditions in which the catalysts are employed, taking in account that the esterification reaction is an active source of H_2O. Through the application of a pressure of 36.2 MPa, self-supported wafers were made with closely 10 mg of each solid, and cropped to a width of 1 cm. The moisture was balanced into an atmospheric stove at 403 K for 24 h, before put it in a high temperature/vacuum chamber 0030-103 from Thermo Scientific (HTVC), configured in this investigation to acquire the transmission FTIR spectra. Each sample into the HTVC device was submitted to a 1.10^{-4} Torr pressure at 403 K for 30 min,

DOI: 10.5281/zenodo.4292694

and then let to cool at room temperature to acquire an FTIR spectrum in absence of pyridine. Then, 6 mmol of dry pyridine was injected into the device to achieve saturation. After 15 min, 50 mL/min of dry N_2 was applied at 403 K for 15 min and then 1.10^{-4} Torr of pressure for 30 min at the same temperature to eliminate the surplus pyridine. This was verified through the repeated acquisition of FTIR spectra until reproducibility. Subsequently, the FTIR spectrum of adsorbed pyridine of each solid was achieved at room temperature. All spectra were performed in a Thermo Scientific Nicolet iS10 spectrometer equipped with an OMNIC Specta software. For the catalytic activity study, 0.150 g each catalyst, were mixed with 0.500 g of oleic acid and 50.0 mL of ethanol 99 %, in a SS Parr 4593 reactor of 100 mL, equipped with a Teflon liner. The esterification reactions were followed for 48 h at 403 K and a fast stirring rate. Aliquots of 3.00 mL of the mixture of each reaction were extracted with a syringe from a lateral port at programmed times. The 3 mL aliquots were cooled and titrated with 0.025 mol/L ethanolic KOH and phenolphthalein as an indicator. The conversion was calculated as (2):

$$X = (Mo\text{-}M)/Mo \quad (2)$$

where Mo and M are the fatty acid concentrations at the beginning and at the t time. The adsorption isotherms of stearic acid at 297 K were performed through a methodology, in which 0.100 g of each solid was shaken with 5 ml of stearic acid 1.10^{-3} mol/L in hexane inside of sealed test tubes. After 24 h, all test tubes were centrifuged and portions of 3 ml from the clear supernatant solution were extracted and titrated with isopropyl KOH 2.10^{-3} mol/L. The amount in mg of stearic acid adsorbed per gram of adsorbent after equilibrium (Qe_0), in the point P_0 of the isotherm was calculated by Eq. (3):

$$Qe_0 = 5\bullet M_{SA}\,(C_0\text{-}Ce_0)/m \quad (3)$$

Where C_0 and Ce_0 are the concentrations in mol/L of stearic acid before and after the equilibrium, M_{SA} is the molar mass in g/mol of the stearic acid and m is the mass in grams of the adsorbent. Every new point P_i (i>0) of the isotherm was obtained after the addition of 3 mL of stearic acid with a growing concentration (Ca_i) from 2.10^{-3} mol/L to 1.10^{-2} mol/L, and repetition of the cycle (shaking, 24 h of waiting and titration) to calculate the next concentrations (C_i) and adsorbed amounts in equilibrium (Qe_i) by Eqs. (4) and (5).

$$C_i = (0.4\ Ce_{i-1} + 0.6\ Ca_i) \quad (4)$$

$$Qe_i = Qe_{i-1} + 5\bullet M_{SA}\,(C_i\text{-}Ce_i)/m \quad (5)$$

The data was adjusted [6] to the Freundlich equation (6):

$$\ln Qe = \ln K_F + 1/n\bullet\ln Ce \quad (6)$$

Where K_F and n are respectively the capacity and the Freundlich intensity of adsorption.

3. Results and Discussion

The ^{27}Al NMR-MAS spectra of the M series (Fig. 1 -A-), shows two main signals close to 55 and 0 ppm, respectively associated [1,2] to framework tetrahedral aluminum (FTA) and octahedral extra-framework aluminum (OEA). At the increasing intensity of the hydrothermal treatment, appears a shoulder close to 30 ppm, associated [7] to condensed extra-framework aluminum species (CEA). The gradual segregation of FTA species out of the crystalline network led to the increase of the total extra-framework aluminum (OEA + CEA) and the diminution of the framework aluminum (Table 1, rows 1 and 2). The ^{27}Al NMR-MAS spectra of Y series (Fig. 1 -B-), show similar behavior, but the extra-framework species, are represented in this case by OEA + CEA and highly symmetric aluminum species (AlO_4^{-5}) probably present in the sodalite box of Y1000 (Table 1, rows 1 and 2). These signals are respectively close to 0, 25, and 90 ppm [8]. The diminution of the ratio between OEA species

DOI: 10.5281/zenodo.4292694

and the total extra-framework aluminum insinuates the transformation of octahedral extra-framework aluminum to other extra-framework species (Table 1, row 3).

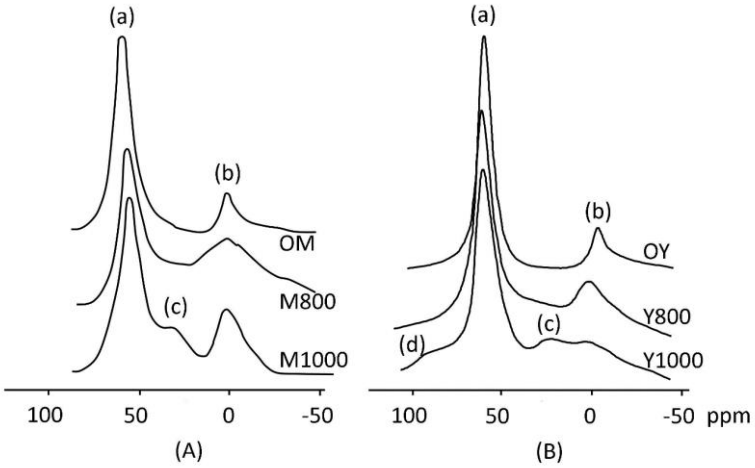

Figure 1. ^{27}Al NMR-MAS spectra of the studied solids. (a) Framework tetrahedral aluminum (FTA), (b) Octahedral extra-framework aluminum (OEA), (c) Condensed extra-framework aluminum (CEA), (d) Highly symmetric aluminum (AlO_4^{-5}).

In the ^{29}Si NMR-MAS spectroscopy of the OM solid (Fig. 2 -A-), the signals in -108.15 and -109.66 ppm have a relationship with units Si(1Al) in different crystalline environments. A third signal centered in -112.99 ppm is probably originated by units Si(0Al). In the spectrum of the solid M800, the signals between -108 and -110 ppm diminish strongly and the signal from the Si(0Al) units is at a higher camp (-114.91 ppm). Finally, two main signals centered on -114.75 and -116.72 ppm in the spectrum of M1000 solid have their most probable origin in Si(0Al) units under different crystalline environments inside the zeolite. On the other hand, the ^{29}Si NMR-MAS spectra of the Y series (Fig. 2 -B-), show the typical look of the faujasite spectra. In both series, the behavior of the spectra agrees with the gradual increase of the Si/Al framework ratio caused by the segregation of tetrahedral aluminum out of the crystalline network, with the increase of the hydrothermal treatment intensity (Table 1, row 4).

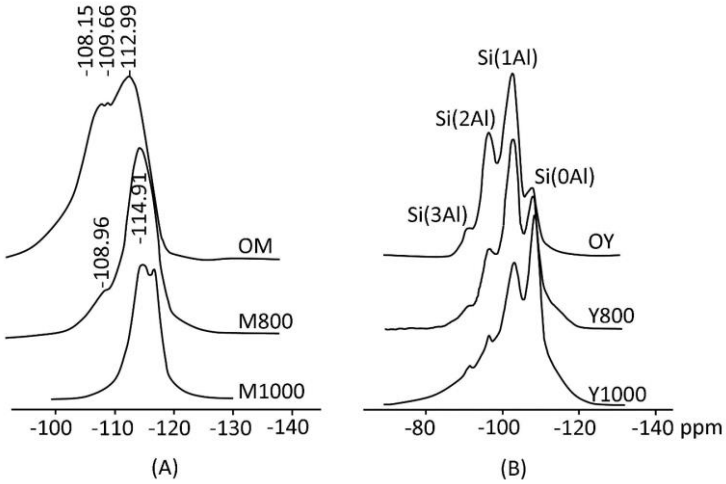

Figure 2. ^{29}Si NMR-MAS spectra of the studied solids.

Table 1. Results of the physical-chemical analysis, catalytic performance, and stearic acid adsorption isotherms.

DOI: 10.5281/zenodo.4292694

SOLID	OM	M800	M1000	OY	Y800	Y1000
***FTA**	83.52	70.73	62.00	86.90	84.61	61.48
***Σ**	16.48	29.27	38.00	13.10	15.39	38.52
OEA/Σ	1	1	0,591	1	1	0,361
Si/Al	6.29	20.81	>>41.27	3.14	4.11	5.13
% Cryst. (XRD)	100	78	59	100	59	37
$X_{48\,h}$	0.909	0.798	0.662	0.753	0.0882	0.0851
Acidity, meq.g^{-1})	2.32	1.34	0.651	2.55	1.75	0.698
n	0.266	2.55	4.01	7.00	7.35	5.53
****K_F**	$5.05 \cdot 10^{-11}$	5.70	18.2	27.0	29.7	17.2
C_B/C_L	1.56	0.29	0.24	1.93	1.48	0.99
TCM *l*	473	453	453	436	433	-
TCM *h*	713	693	653	656	653	634

*Percentages concerning the total extra-framework aluminum (OEA+CEA+AlO_4^{-5}) ∑ and the framework tetrahedral aluminum (FTA). **[(mg/g)/(mg/L)$^{1/n}$]. (TCM), the temperature of the center of mass calculated through the integrated areas below the *l* and *h* branches.

The completion of the FTIR spectroscopy of pyridine adsorption study on incipient moisture conditions allowed reproducing approximately the conditions in which the catalysts are employed, taking into account the esterification reaction in itself is an active source of de H_2O. Predictably, the presence of water led to some broadening of the signals because of the hydrogen bonding. However, it was possible to see relevant aspects of the general behavior of the infrared bands from the pyridine and water adsorption, between 1400 and 1700 cm^{-1}. The identification of the infrared signals from the spectrum of pyridine adsorbed on acid sites was possible through a careful review of the related bibliography [3,4,5]. The infrared study of adsorbed pyridine on the M series (Fig. 3 –A-) shows that signals centered at 1636 cm^{-1} and 1540 cm^{-1} (from pyridinium ion resultant of the adsorption on the Brönsted acid sites) are smaller in solids treated at stronger hydrothermal conditions.

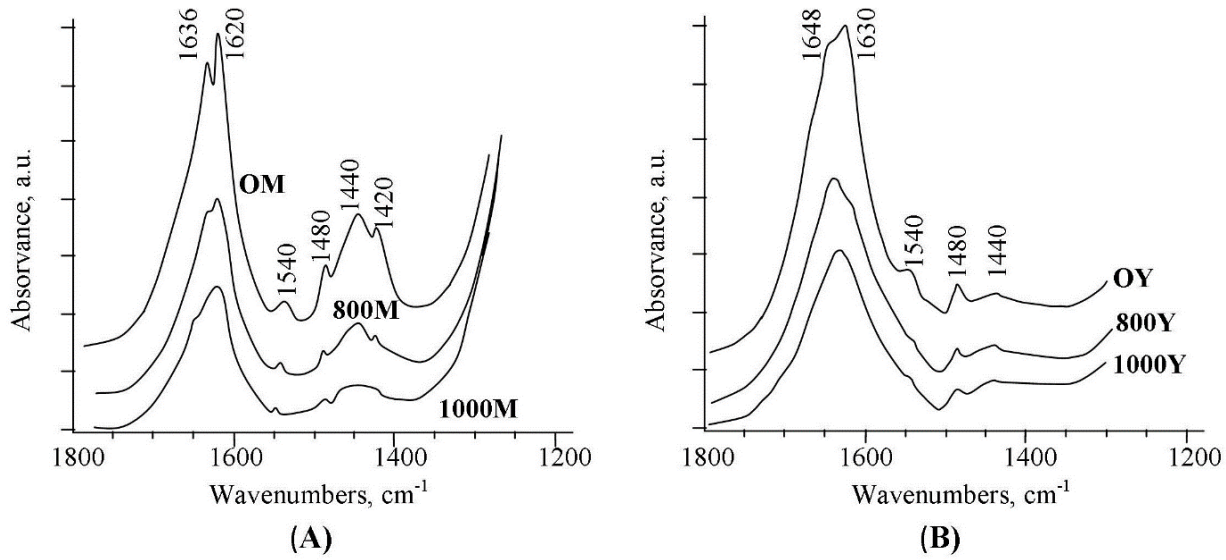

Figure 3. FTIR spectra of pyridine adsorption on incipient moisture conditions.

DOI: 10.5281/zenodo.4292694

This result matches with the diminution of the bridged Si-OH–Al groups (associated with the Brönsted acidity) by the segregation of the tetrahedral aluminum out of the crystalline framework because of the hydrothermal treatment. Also, it can see the diminution of the signal associated with pyridine coordinately bonded to Lewis acid sites, centered in 1440 cm^{-1}. Another signal at 1620 cm^{-1} is overlapped with the H-O-H bending mode frequency. The spectroscopy ^{27}Al NMR evinces the diminution of the ratio between OEA species and the total extra framework aluminum (Table 1, row 3), suggesting the conversion of the octahedral extra-framework aluminum (Lewis-associated) in non-acidic extra-framework species. Then the signal centered at 1480 cm^{-1}, resultant of signals overlapping of the pyridinium ion and coordinately bonded pyridine, decreases by the described changes in the nature of the aluminum species. The diminution of the signals at 1420 cm^{-1} (hydrogen-bonded pyridine) and 1620 cm^{-1} (mainly bending vibrations of physisorbed water) point out the diminution of the polar character and the increase of the hydrophobicity because of the segregation of the tetrahedral aluminum out of the crystalline framework. The spectra from the pyridine adsorbed on the Y series let to see similar behavior, even though they have lesser resolution than spectra from the M series (Fig. 3 -B-): the infrared spectra show the decrease of the peaks resulting from the pyridine adsorption on Brönsted acidic sites at 1540 cm^{-1} and the Lewis acidic sites at 1450 cm^{-1}; as well as the signal centered at 1480 cm^{-1}, associated with the pyridine chemisorption on both types of acid sites. As in the M series, this behavior accords with the growing segregation of the tetrahedral aluminum and the transformation of the octahedral extra-framework aluminum in non-acidic extra-framework species as a result of the hydrothermal treatment. The region between 1600 and 1650 cm^{-1} follow the same decreasing pattern showed by the remaining signals: It is possible to distinguish two signals close to 1648 cm^{-1} (associated with the pyridinium ion) and 1630 cm^{-1} (from the overlapping of the H-O-H bending of physisorbed water and the coordinately bonded pyridine). This implies a little displacement to higher frequencies than the M series, suggesting lesser acidic strength. Assuming that the signal near 1630 cm-^{1} has the H-O-H bending of physisorbed water as the main component, its diminution with the hydrothermal conditions accords with the hydrophobicity increase because of the segregation of the tetrahedral aluminum out of the crystalline framework. The variability, often caused by very subtle differences in the experimental conditions, between the reported values of the extinction coefficients ϵ_B and ϵ_L, respectively based on the absorbances of the bands around 1545 cm^{-1} (pyridinium ion bonded to Brönsted sites) and 1455 cm^{-1} (pyridine adsorbed on Lewis acid sites) led to use of the ϵ_L/ϵ_B ratio (which is less sensitive to changes in the experimental conditions). The C_B/C_L concentration ratio between Brönsted and Lewis acid sites was calculated through the equation (7) [3]:

$$C_B/C_L = (\epsilon_L/\epsilon_B).(A_B/A_L) \quad (7)$$

Where A_B/A_L is the absorbance ratio between the bands around 1545 and 1455 cm^{-1}. Under these considerations, the value of ϵ_L/ϵ_B = 0.88, derived from the studies performed by Selly and Forni [9] was used as an adequate value for the determination of the C_B/C_L ratio. A comparison between solids submitted to the same hydrothermal treatment conditions (OM-OY, M800-Y800, and M1000-Y1000) in both series, reveals that C_B/C_L values are significantly higher in the Y than the M series (Table 1, row 10), agreeing with a higher density of Brönsted than Lewis acid sites in the Y series. Another important aspect of these results is the continuous decrease of the C_B/C_L ratio in both series, at increasing conditions of the hydrothermal treatment. This indicates a faster diminution of Brönsted than Lewis acidity because of the gradual transformation of the framework tetrahedral aluminum into extra-framework aluminum species, as the result of the hydrothermal treatment. However, as the ^{27}Al NMR spectroscopy suggested, the octahedral extra-framework aluminum (associated with the Lewis acidity) suffers a partial transformation into non-acidic extra-framework species.

DOI: 10.5281/zenodo.4292694

The TPD-NH_3 profiles from the M and Y series (Fig. 4) show two differentiated zones, corresponding to lesser (*l*-branch) or higher (*h*-branch) desorption temperatures than 573 K [3]. While there is consensus about that *h*-branch comes from desorption of NH_3 bonded to superficial acid sites, there is a persisting controversy about the origin of the *l*-branch [10,11,12].

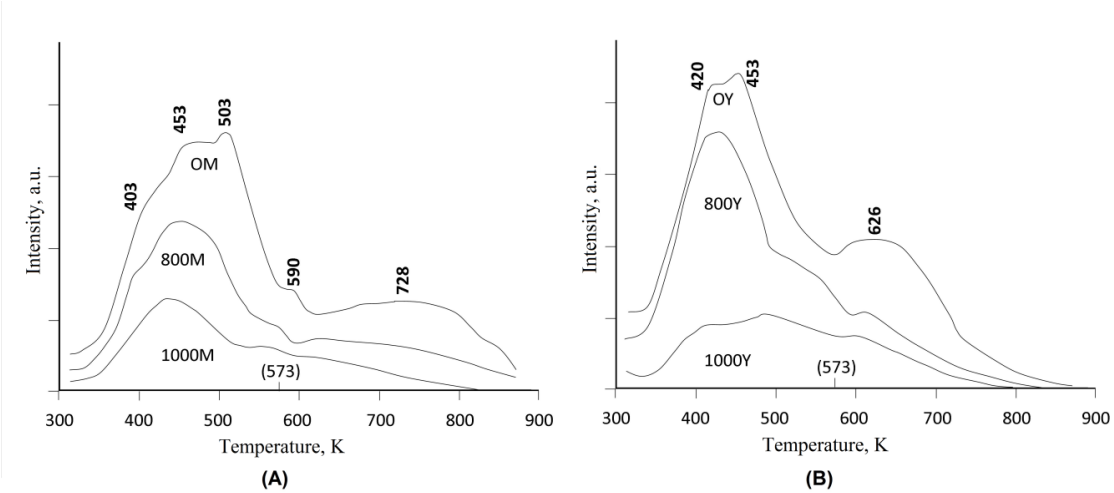

Figure 4. The TPD-NH_3 profiles from the M and Y series.

However, results from this investigation show that *l* and *h* branches diminish at stronger hydrothermal treatment conditions where the Si/Al ratio increases due to the segregation of the tetrahedral aluminum (FTA) out of the crystalline framework, with the subsequent diminution of the Brönsted acidity. The FTIR spectroscopy shows that Lewis acidity also diminishes, probably because of the conversion of the octahedral extra-framework aluminum (OEA) into non-acidic extra-framework species, suggested by ^{27}Al-NMR. Consequently, the relation between the *l*-branch and the acidity cannot be discarded. A possible origin for the *l*-branch is NH_3 physically adsorbed on ammonium ions resulting from chemisorbed ammonia molecules on the acid sites or the direct desorption of NH_3 from superficial weak acid sites. Similar considerations were exposed by researchers as Lónyi and Valyon [13]. The M series profiles (Fig. 4 -A-), show the diminution of the area below them at the increasing intensity of hydrothermal treatment conditions, with a more accentuated diminution of the *h*-branch, suggesting a faster diminution of stronger than weaker acid sites. The shape of the TPD-NH_3 profile evinced sites with different acid strength: Shoulders close 403 K and 590 K disappear gradually at stronger hydrothermal conditions. A shoulder centered close to 453 K (in the OM solid) is substituted by a summit in M800 and M1000, whereas a signal around 503 K vanishes with the hardening of the hydrothermal conditions. Likewise, a wide signal centered close to 728 K in the OM solid, is caused by strong acid sites, but M800 and M1000 solids scarcely show a signal at that temperature. An additional aspect is a general trend of the desorption signals and the "temperature of the center of mass" (TCM) calculated from the integrated areas below the *l* and *h* branches to move to lesser temperatures at stronger hydrothermal conditions of treatment, evincing the progressive diminution of the acidic strength (Table 1, rows 11 and 12). The TPD-NH_3 profiles from the Y series (Fig. 4 -B-) show prominent signals close to 420 K (shoulder in OY), 453 K, and 626 K which intensity diminishes at increasing hydrothermal treatment strength in order OY > Y800 > Y1000. Similarly to the M series, there is a more accentuated diminution in the *h*-branch than the *l*, suggesting a faster diminution of the stronger than the weaker acid sites. Also, signals move to lesser temperatures at increasing hydrothermal treatment strength, pointing out to the progressive diminution of the acidic strength. In the Y1000 solid, the heterogeneous nature of its acid sites does not allows recognizing a concrete pattern and scarcely shows a signal at a high-temperature zone

DOI: 10.5281/zenodo.4292694

as a consequence of a depth collapse of the structure due to the high-temperature hydrothermal treatment. A comparison between solids submitted to the same hydrothermal treatment conditions shows that TCM values are higher in M than the Y series; evincing that the mean acid strength is higher in the M than the Y series (Table 1, rows 11 and 12). However, the density of acid sites is higher in the Y series than in the M series (Table 1, row 7). The increase of the Si/Al ratio caused by the segregation of the tetrahedral aluminum out of the crystalline framework because of the hydrothermal treatment leads to the diminution of polar Si-OH-Al groups associated with the Brönsted acidity and the increase of extra-framework species. This situation leads to an increase in the hydrophobicity and the diminution of the net acidity. A preliminary inspection of the stearic acid adsorption isotherms (Fig. 5) shows that steamed solids from the M series (M800 and M1000) have a greater affinity to stearic acid than the Y series.

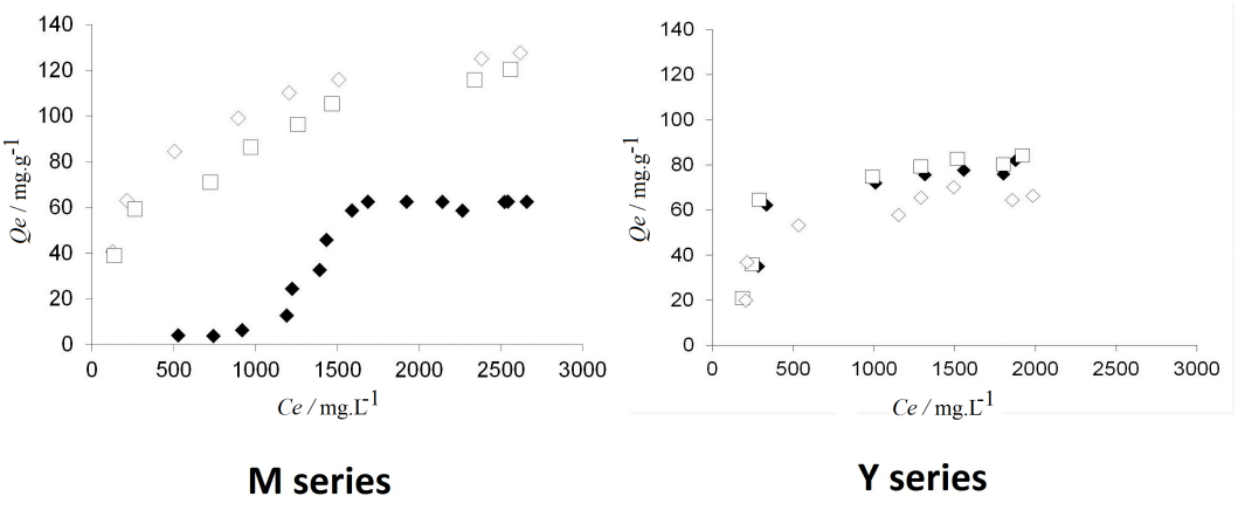

Figure 5. Adsorption isotherms of stearic acid. Left: •) OM, □) M800 and ◊) M1000. Right: •) OY, □) Y800, and ◊) Y1000.

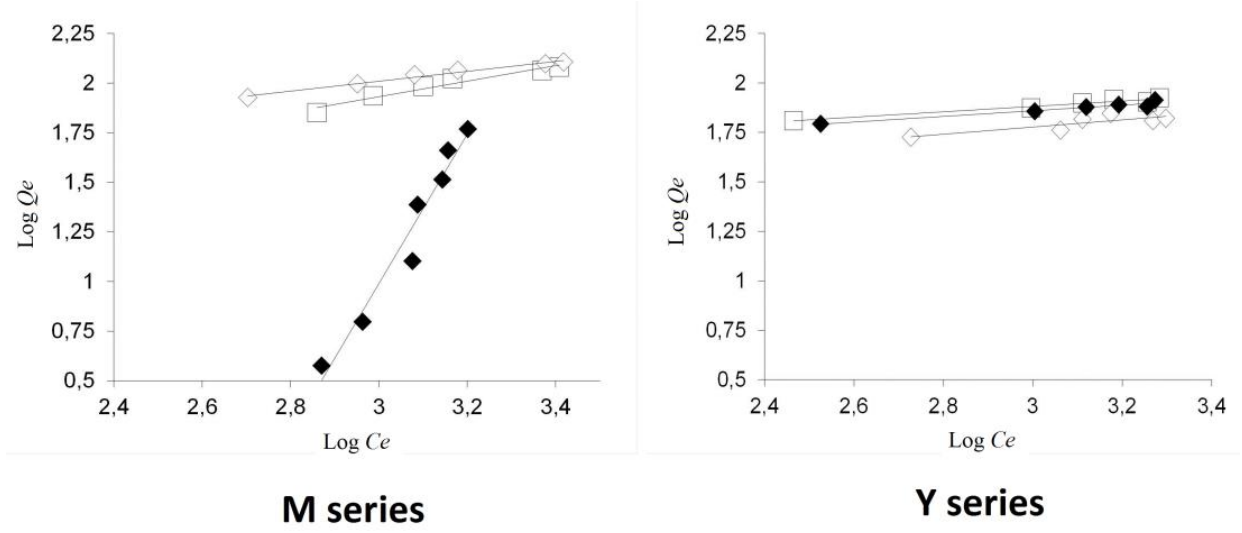

Figure 6. Adjustment of the adsorption isotherms of stearic acid to the Freundlich equation. Left: •) OM, □) M800 and ◊) M1000. Right: •) OY, □) Y800, and ◊) Y1000.

DOI: 10.5281/zenodo.4292694

The adjustment of the data from the M series to the Freundlich equation (Fig. 6 -Left-), reveals greater affinity between the fatty acid molecules and solids treated at stronger hydrothermal conditions; as is deduced from the continuous increment of the parameters K_F and n (Table 1, rows 8 and 9). Unlike that behavior, the stearic acid adsorption isotherms on OY and Y800, almost coincide (Fig. 5 -Right-) and show a slightly greater affinity to stearic acid than Y1000. That reflects on the parameters K_F and n (Table 1, rows 8 and 9) from the adjustment to the Freundlich equation (Fig. 6 –Right-). These results suggest two different ways of adsorption of free fatty acid molecules (FFA) on the surface of the studied series. In the M series, with a low-density of bridged Si-OH-Al sites, adsorption mainly occurs on the external surface, by London forces on slightly polar sites in a tight arrangement (Fig. 7 -A-). Likewise, the adsorption by hydrogen-bonding (Fig. 7 -B-) is probably less frequent. Then, whenever the number of slightly polar sites grows by the effect of the hydrothermal treatment, the number of adsorbed FFA molecules increases leading to increasing values of K_F and n. In the Y series, with a high-density of bridged Si-OH-Al sites, a significant part of adsorbed FFA molecules probably is hydrogen-bonded to the bridged OH sites (Fig. 7 -B-) on the inner surface of the channels and the alpha cage, where the tight adsorption in a perpendicular arrangement is not possible.

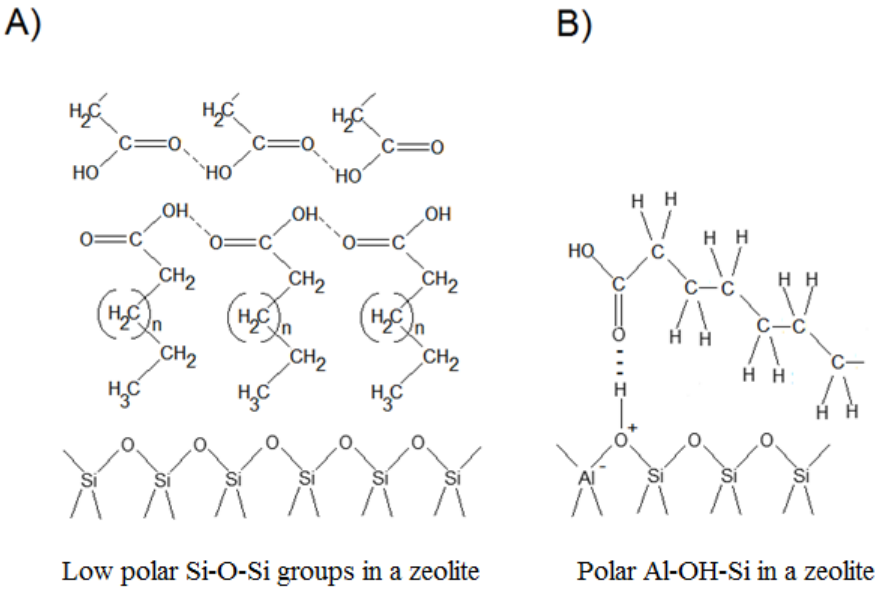

Figure 7. Possible adsorption ways of the fatty acid molecules: (A) Through London dispersion forces. (B) Through hydrogen bonding.

Moreover, in a high-density situation, tails of hydrogen-bonded FFA molecules can overlap mutually (Fig . 8), creating an interwoven that would encumber the adsorption of new FFA molecules on the external surface. Therefore, growing the number of slightly polar sites at increasing conditions of the hydrothermal treatment would have little effect on the number of adsorbed FFA molecules, leading to similar values of K_F and n. On the other hand, the diminution of the adsorption capacity of the Y1000 solid can be a consequence of the significant structural collapse resulting from the high-temperature hydrothermal treatment.

DOI: 10.5281/zenodo.4292694

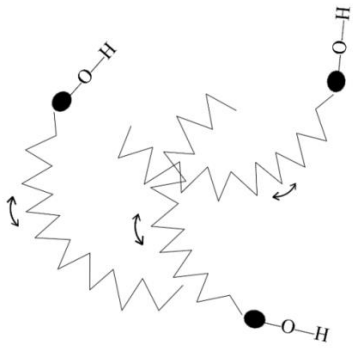

Figure 8. Upper idealized view from hydrogen-bonded free fatty acid (FFA) molecules on the zeolite surface, in a high-density situation. "●": Hydrogen-bonded carbonyl functions from FFA molecules.

Furthermore, the prevailing of K_F values in the Y series solids regard their counterparts of M series point that adsorption of FFA molecules by hydrogen bonding on the bridged OH sites (predominant in the Y series) is stronger than adsorption on slightly polar sites by London forces. The X-ray diffraction (Fig . 9) exposes the progressive diminution of the relative crystallinity. This agrees with the reduction of the characteristic peaks in mordenites [14] close to 9.8, 22.4, 25.8 and 26.4° of 2θ and the characteristic peaks in faujasites [15], close to 15.8, 18.9, 20.5, 23.8, 27.2, 30.9, 31.6 and 34.3º of 2θ (Table 1, row 5); as a result of the growing collapse of the crystalline network by the hydrothermal dealumination. The conversion from oleic acid to ethyl ester follows the general decreasing trend shown by the relative crystallinity and the densities of the acid sites (Table 1, rows 5-7).

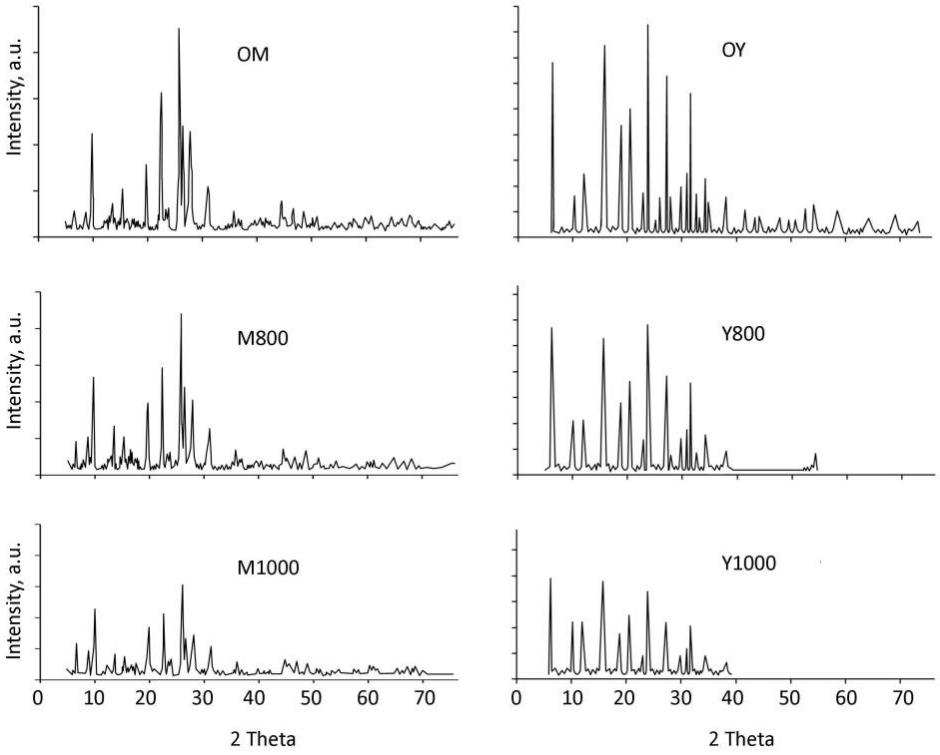

Fig . 9. Diffraction patterns of the studied solids.

DOI: 10.5281/zenodo.4292694

This behavior agrees with the gradual increase of the Si/Al framework ratio and the diminution of the bridged Si-OH–Al groups (associated with the Brönsted acidity) caused by the segregation of the tetrahedral aluminum (FTA) out of the crystalline framework (Table 1, rows 1 and 4), with the increase of the hydrothermal treatment intensity. Moreover, the presence of stronger acid sites in the M than Y series (evinced by TPD-NH_3) can explain the general tendency of higher catalytic activity in the M series than the Y series of solids submitted to the same hydrothermal treatment conditions. Superior acidic strength in mordenites than faujasites and MFI zeolites was previously reported by Kapustin *et al* [16].

4. Conclusions

Results confirm that the leaving of tetrahedral aluminum out of the crystalline network, lead to the increase of the hydrophobicity and the creation of new sites with lesser polarity. Additionally, these results suggest that the FFA molecules are adsorbed in two principal manners for each zeolite type. In mordenites with a low-density of bridging Si-OH–Al groups, most of the adsorbed FFA molecules are probably adsorbed through London dispersion forces onto the less polar sites with its carboxyl groups oriented away from the zeolitic surface in a tight arrangement. This drives the increase of the adsorption of FFA molecules with the increase of the Si/Al ratio. Conversely, in the studied faujasites, the higher density of bridging groups favors the adsorption of a significant fraction of FFA molecules with their carboxyl group hydrogen-bonded to the more polar Si-OH–Al groups, leading to the decrease of the adsorption of FFA molecules as the Si/Al ratio increases. On the other side, in both zeolite types, the diminution of acid sites density is the principal cause of the diminution of the esterification activity.

Acknowledgments

The author thanks Dr. Carmen M. López -CCPP-UCV- (For providing the zeolites Na-MOR and Na Y) and Dr. Joaquín Brito –IVIC- (For providing the XRD and NMR techniques).

References

1. G. Giannetto, A. Montes and G. Rodríguez. Zeolitas (2nd ed), Editorial Innovación tecnológica, Caracas, 2000. (ISBN 980-00-1648-1)
2. H. van Bekkum, E.M. Flanigen, P. Jacobs and J.C. Jensen in Introduction to Zeolite Science and Practice (2nd ed), Elsevier, New York, 2001. (ISBN 0444-82421-9)
3. L.F. Isernia, Materials Research. 16 (2013) 792. (https://doi.org/ 10.1590/S1516-14392013005000044)
4. N.Y Topsøe, K. Pedersen, E.G. Derouane, Journal of Catalysis. 70 (1981) 41. (https://doi.org/10.1016/0021-9517(81)90315-8)
5. J. Fang and L. Yongdan, Catalysis Today. 145 (2009) 101. (http://dx.doi.org/10.1016/j. cattod.2008.06.007)
6. H. Freundlich, Phisik. Chem. 57 (1907) 385.
7. M.A. Zanjanchi, M. Mohammadi, J. Sci. Islam. Repub. Iran 12 (2001) 113.
8. C.P Gray in: Scott M. Auerbach, K.A. Carrado and P.K. Dutta (Eds.), Nuclear Magnetic Resonance Studies of Zeolites 2003, Handbook of Zeolite Science and Technology of Marcel Dekker, New York, 2003. (ISBN 0-8247-4020-3)
9. E. Selly and R. Forni, Microporous and Mesoporous Materials. 31 (1999) 129.
10. Q. Zhao, W.H. Chen, S.J. Huang, Y.C. Wu, H.K. Lee, and S.B. Liu, The Journal of Physical Chemistry. 106 (2002) 4462. (ttp://dx.doi.org/10.1021/jp015574k54)

DOI: 10.5281/zenodo.4292694

11. D. Ma, W.P. Zhang, Y.Y. Shu, X.M. Liu, YD. Xu, and X.H. Bao, Catalysis Letters. 66 (2000) 155. (http://dx.doi.org/10.1023/A:101909960702956)
12. M. Iwasaki, K. Yamazaki, K. Banno, and H. Shinjoh, Journal of Catalysis. 260 (2008) 205. (http://dx.doi.org/10.1016/j.jcat.2008.10.009)
13. F. Lónyi and J. Valyon, Microporous and Mesoporous Materials. 47 (2001) 293. (https://doi.org/10.1016/s1387-1811(01)00389-4).
14. S. Kulawong, S. Prayoonpokarach, A. Neramittagapong, and J. Wittayakun, Journal of Industrial and Engineering Chemistry. 17 (2011) 346. (https://doi.org/10.1016/j.jiec.2011.02.037)
15. ASTM D3906 - 03 (2013). Standard Test Method for Determination of Relative X-ray Diffraction Intensities of Faujasite-Type Zeolite-Containing Materials. (https://doi.org/10.1520/d3906-03r08)
16. G.I. Kapustin, T.R. Brueva and I.V. Mishin, 12th International Zeolite Conference. Materials Research Society. (1999) 2637.